A Study Using X-ray Absorption and Emission Spectroscopy of Dioxygen-Binding Xerogels Incorporating Cyclam Units Complexed with Copper Salts

José Goulon,*[a] Chantal Goulon-Ginet,[a,b] Andrei Rogalev,[a] Fabrice Wilhelm,[a] Nicolas Jaouen,[a] Delphine Cabaret,[c] Yves Joly,[d] Géraud Dubois,[e,f] Robert J. P. Corriu,[g] Gabriel David,[e] Stéphane Brandès,[e] and Roger Guilard*[e]

Keywords: X-ray absorption spectroscopy / Tetraazamacrocyclic ligand / Dioxygen binding / Peroxo ligand / Copper

X-ray absorption spectroscopy was used to elucidate how hybrid xerogels complexed with $CuCl_2$ could reversibly bind molecular dioxygen. Difference EXAFS analyses at the Cu K-edge suggest that dioxygen could bridge two Cu atoms in a μ-η^1:η^1 peroxo-like conformation with unequal Cu···O distances. Only the short distance (R_{Cu-O1} = 1.86 ± 0.01 Å) was unambiguously determined and looks typical of a Cu^{II} site. The Cu···Cu internuclear distances would be rather long: $R_{Cu-Cu} \approx 4.0$ Å (3.9 Å) for the oxygenated (oxygen-free) xerogels. Cl K-edge EXAFS spectra revealed the pre-existence in the oxygen-free xerogels of Cu^{I} sites with short Cl–Cu bonds (2.11 ± 0.03 Å). Pentacoordinate Cu^{II} sites with a longer Cl–Cu bond (2.45 ± 0.03 Å) were also identified. Another signal at a further distance (2.73 ± 0.03 Å) suggests that the Cl ions could bridge mixed-valence $\{Cu^{I},Cu^{II}\}$ sites. In oxygenated xerogels complexed with $CuCl_2$, ca. 75% of the Cu atoms would be singly bound to dioxygen while the signature of the pentacoordinate Cu^{II} sites would totally vanish. Substituting $CuBr_2$ for $CuCl_2$ yields xerogels with a poor capability to bind dioxygen. This is remarkably correlated with a decrease of the signatures at R_{Cu-O1} = 1.86 Å and R_{Cu-Cu} = 4.0 Å. EXAFS spectra of the oxygen-free xerogel complexed with $CuBr_2$ again exhibit signatures assigned to short (2.30 Å)/long (2.49 Å) Cu–Br bonds as expected for mixed-valence $\{Cu^{I},Cu^{II}\}$ systems. Inactive xerogels prepared with metallated cyclams seem to undergo a structural change during hydrolysis and polycondensation. Deconvoluted XANES spectra of the active xerogels exhibit a strong pre-edge resonance which is characteristic of mixed-valence Cu^{I} sites. This interpretation was supported by ab initio XANES simulations carried out beyond the muffin-tin approximation.

Introduction

In the past decade, nanostructured organic-inorganic hybrid polymers have attracted much attention because these novel materials offer unique combinations of optical, physical[1,2] or chemical[3–5] properties. It was a stimulating challenge for chemists to prepare hybrid polymers chelating metal cations in such a way that the metal would still be accessible for catalytic activity. Starting from the consideration that saturated polyazamacrocycles, especially the 1,4,8,11-tetraazacyclotetradecane (cyclam), had a strong capability to bind transition metal cations,[6–10] two partner groups (located in Dijon and Montpellier) settled upon incorporating cyclam units within silica matrices prepared by a sol-gel process.[11–13] Two strategies illustrated in Scheme 1 were explored:[13]

(A) The hydrolysis and polycondensation of $[Cu(cyclam)]^{2+}$ or $[Co(cyclam)]^{2+}$ alkoxysilylated complexes quantitatively produced hybrid polymers incorporating the metallated cyclam units.

(B) The hydrolysis and polycondensation of the alkoxysilylated (uncomplexed) cyclam precursors was performed first and the metal salt (e.g. $CuCl_2$) was then incorporated into the hybrid xerogel (Scheme 1).

Interestingly, it was found that, in the case of $CuCl_2$, the materials prepared by routes (A) and (B) had different spectrochemical properties reflecting different structures. Typically, xerogels of type (A) had a strong X-band EPR signal at 3200 G with a broad linewidth ($g \approx 2.15$) at room tem-

[a] European Synchrotron Radiation Facility,
B. P. 220, 38043 Grenoble Cedex, France
E-mail: goulon@esrf.fr
[b] Université J. Fourier, Faculté de Pharmacie,
38706 La Tronche, France
[c] Universités Paris VI et VII, Laboratoire de Minéralogie-Cristallographie associé au CNRS,
4 place Jussieu, 75252 Paris Cedex 05, France
[d] Laboratoire de Cristallographie du CNRS, associé à l'Université J. Fourier,
B. P. 166, 38042 Grenoble Cedex 9, France
[e] Laboratoire d'Ingénierie Moléculaire pour la Séparation et les Applications des Gaz, UMR 5633, CNRS, Université de Bourgogne, Faculté des Sciences Gabriel,
Boulevard Gabriel, 21100 Dijon, France
[f] Present address: IBM Almaden Research Center,
650 Harry Road, San Jose, CA 95120, USA
[g] Université de Montpellier II, Laboratoire de Chimie Moléculaire et Organisation du Solide, UMR 5637, CNRS,
Place E. Bataillon, 34095 France
Supporting information for this article is available on the WWW under http://www.eurjic.org or from the author.

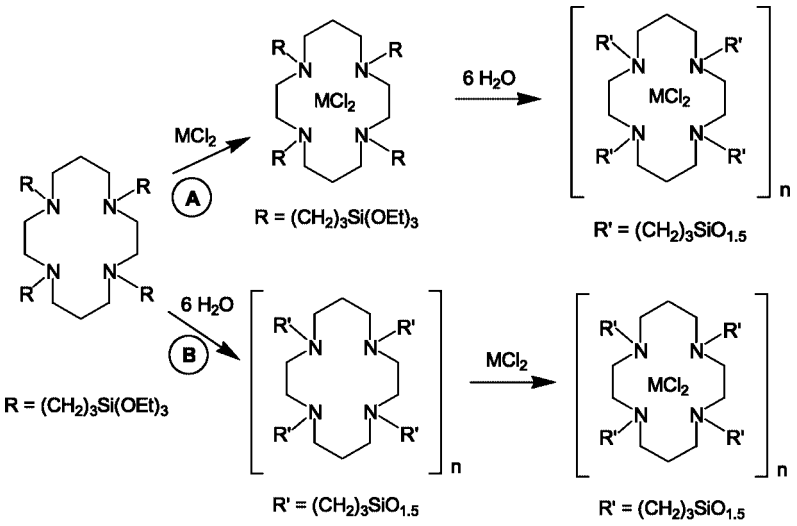

Scheme 1. Alternative routes to yield metallated hybrid xerogels following Route (A) and Route (B).

perature and at 100 K. This signal was assigned to Cu^{II} centers, but this broad signal vanished for xerogels of type (B). In contrast, xerogels of type (B) exhibited a much weaker signal at 1550 G ($g \approx 4.40$), which often characterizes dicopper interactions associated with a dinuclear structure. What made this structural problem even more interesting was the discovery that xerogels prepared by route (B) could bind (and possibly activate) molecular dioxygen whereas xerogels prepared by route (A) were essentially inactive. Recent tests have confirmed that the ability of xerogels of type (B) to bind dioxygen would be as high as for hemocyanin (Hc).

We tried to elucidate the puzzling structure of xerogels of type (B) using X-ray absorption and the XANES spectra were compared with ab initio simulations performed with an advanced code (FDMNES) that offered a double benefit. First, we could control the charge transfer from the ligand toward the metal, this option being useful here to describe the contribution of the neutral cyclam ligands. Second, we were not constrained to using spherically averaged muffin-tin potentials as with standard codes. The latter advantage is particularly sensible for covalent bonding.

Results and Discussion

Coordination Geometry: EXAFS Studies

The structural information contained in EXAFS spectra is often difficult to decipher. Analyses become most delicate when destructive interferences cause major spectral distortions and a loss of information.[14,15] Global fits can be either misleading or simply unreliable due to large correlations. Even with such complicated problems, the strength of EXAFS stems from its very high sensitivity to small structural changes and this is precisely what we tried to exploit with difference analyses. It is indeed recommended that the consistency of the analyses be checked by combining EXAFS spectra collected adifferent absorption edges.

EXAFS analyses of model compounds **1** = Cu(TPP), **3** = $[Cu(tmc)](BF_4)_2$ and **6** = [Cu(tpc)Cl]Cl are detailed only in the supporting information section. This preliminary study was very helpful because it made the limits of a direct data reduction fully transparent even though high quality data were collected over a wide spectral range. Given the highly symmetrical (D_{4h}) geometry of the copper porphyrin, the FT spectra of **1** offer a rich pattern of signatures which justified refined analyses, taking the multiple scattering paths into account. In contrast, the poor rigidity of the 14-membered saturated macrocyclic ligand restricted the information that could be extracted from the EXAFS spectra of complexes **3** and **6**. In the hexacoordinate species **3**, dynamic distortions of the axial and equatorial bonds can be predicted from the Jahn–Teller theorem[16] and were found to cause significant spectral distortions. Compound **6** was initially expected to be pentacoordinate, the copper ion being shifted away from the average plane of the four nitrogens with some trigonal distortion also arising from the ligand field. Published crystal structures of related pentacoordinate Cu complexes[17–19] raised a troublesome question regarding the true chemical formulation of compound **6**. Such pentacoordinate complexes were systematically found to be mixed-valence complexes due to the presence of linear anions $[Cl{-}{-}{-}Cu^{I}{-}{-}{-}Cl]^{-}$. The problem is that EXAFS is critically sensitive to the presence of such anions in which the short Cu^{I}–Cl bond (2.116 Å) is comparable to the Cu^{II}–N bond (2.13 Å). Destructive interferences between these two EXAFS signals are expected, the practical result being a loss of intensity of the Cu---N signature. This is a typical circumstance where, in our experience, analyses based only on fits would dangerously fail because the mathematical problem is poorly defined.[14,15] In combining the EXAFS spectra of species **6** recorded at both the Cu and Cl K-

edges, we could produce strong evidence of the contributions of the linear anion $[Cl{-}{-}{-}Cu^{I}{-}{-}{-}Cl]^{-}$. This was received as a strong warning that standard fitting procedures may not be suitable to analyze the EXAFS spectra of our xerogels.

Active Xerogels Complexed with $CuCl_2$

In this paper, reactive materials towards dioxygen binding will be considered as "active" systems while unreactive solids in an ambient atmosphere will be called "inactive". Our strategy was first to compare the Cu K-edge FT EXAFS spectra of the oxygenated xerogel **XB2** with the oxygen-free xerogel **XB1**, both xerogels being complexed with $CuCl_2$. The relevant FT spectra $Im\tilde{\chi}_N(R)$ are displayed in Figure 1A. For model compound **3**, the FT spectra exhibit strong signatures which can be assigned unambiguously to the {Cu···N} and {Cu···Cα1} single scattering paths involving the cyclam ring with R_{Cu-N} = 2.02(2) Å and $R_{Cu-C\alpha1}$ = 2.8(8) Å. Since these signatures are nicely superimposed for the two xerogels, we were led to the first conclusion that the coordination geometry of the cyclam macrocycle can hardly be heavily altered in the oxygenated xerogel **XB2**. It thus became attractive to envisage difference analyses. We have reproduced in Figure 1B the FT spectra $Im\tilde{\chi}_N(R)$ and $|\tilde{\chi}_N(R)|$ obtained by Fourier transforming the difference EXAFS signal of a virtual species [**XB2-XB1**].

The most striking feature in Figure 1B is a sharp, nicely resolved peak which we assigned to a short Cu–O1 bond. The corresponding distance would be much too short to reflect any realistic distortion of the cyclam macrocycle. This led us to incorporate the phase shifts and scattering amplitudes of a Cu···O shell, calculated with FEFF8.9 for a cluster that has the structure of a well-characterized Cu–dioxygen model compound, into the optical FT.[20] Then by using a standard single shell fit, we could refine the distance: R_{Cu-O1} = 1.855 ± 0.005 Å, the Debye–Waller factor: $[\sigma_{Cu-O1}]^2$ = 0.00086 Å^2 and the average number density of bound oxygen atoms: N_{Cu-O1} = 0.76 ± 0.06 per copper site. The distance R_{Cu-O1} is much shorter than any Cu^{II}–OH bond length (1.97–2.02 Å) in copper hydroxyhalide minerals[21–25] like atacamite, paratacamite or in active phases of supported catalysts used for oxychlorination of ethylene.[26–28] In contrast, our R_{Cu-O1} distance compares remarkably well with the Cu–O bond lengths of Cu–dioxygen complexes of known crystal structures.[29,30] For instance, it is very close to the distance R_{Cu-O1} = 1.852 Å or R_{Cu-O1} = 1.868 Å found respectively in the end-on dinuclear μ-*trans* peroxo dicopper complex of Karlin[31,32] and Susuki[33] in which the dioxygen molecule is bound to two copper sites. If we accept that this may also be true for xerogel **XB2**, then our fit led us to expect the fraction of bound dioxygen molecules per copper site to be of the order of ca. 38%. It is quite remarkable that this value is nicely consistent with earlier measurements of oxygen adsorption which had established that the fraction of bound dioxygen should be near 40%. Note that the Cu···O1 signal could be seen directly in the FT spectrum of xerogel **XB2** displayed in Figure 1(A). Unfortunately, it interferes with the negative sidelobe of the intense Cu···N signal that makes the assignment problematic.

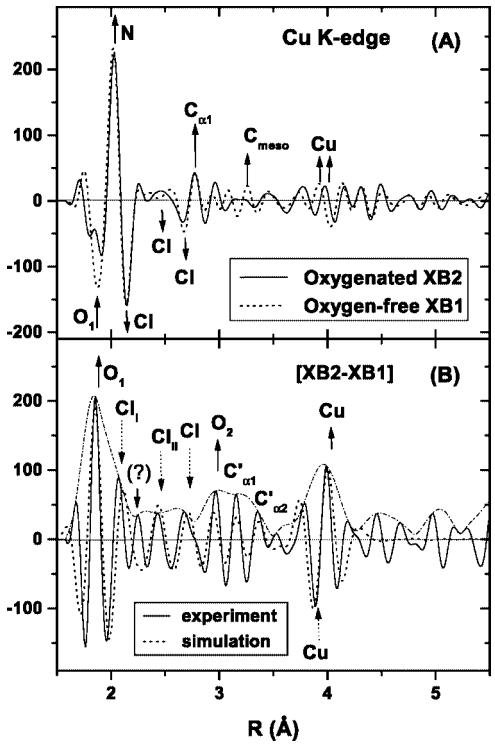

Figure 1. (A) Comparison of the Cu K-edge FT spectra $Im\tilde{\chi}(R)$ of xerogel **XB2**$[CuCl_2]/O_2$ (solid line) and of xerogel **XB1**$[CuCl_2]/N_2$ (dotted line). Arrows indicate where weak contributions of bridging chloride ions may interfere in xerogel **XB1**. (B) Cu K-edge FT spectra $Im\tilde{\chi}(R)$ (solid line) and $|\tilde{\chi}(R)|$ (dot-dashed line) of the difference signal of [**XB2** (oxygenated) – **XB1** (oxygen-free)]. A simulated FT difference EXAFS spectrum $Im\tilde{\chi}(R)$ (dotted line) is also reproduced which was calculated using a structure derived from Figure 3(A).

In the difference FT spectrum $|\tilde{\chi}_N(R)|$ shown in Figure 1B, there is another strong signature peak near 4 Å. We have assigned this signal to the derivative of a single scattering Cu···Cu EXAFS signal, resulting from a small variation of the distance R_{Cu-Cu} when dioxygen is bound to copper. At this stage, we would like to stress that this signal cannot be an experimental artefact since it is present in all difference analyses performed with individual scans. Clearly, the assignment of such a weak Cu···Cu EXAFS signal in the FT spectra displayed in Figure 1(A) would again be problematic because it is feared that this signal could interfere with the intense contributions of multiple-scattering paths involving the nitrogen atoms of the cyclam ligand. This is where a difference analysis can offer a decisive simplification of the spectra. Based on our experience, only a heavy scatterer like a copper atom could give such a strong signature at a long distance in the FT difference spectrum.

A simulation of the difference spectrum that is also reproduced in Figure 1(B) supports our interpretation. Using phase-shifts and scattering amplitudes calculated with

FEFF8.9 for the same Cu–dioxygen model compound,[20] the best agreement was obtained for $R_{Cu-Cu} = 3.99 \pm 0.03$ Å; $[\sigma_{Cu-Cu}]^2 = 0.0032$ Å^2 in the oxygenated xerogel **XB2**; $R_{Cu-Cu} = 3.89 \pm 0.02$ Å; $[\sigma_{Cu-Cu}]^2 = 0.0032$ Å^2 in the oxygen-free xerogel **XB1**. The number density $N_{Cu-Cu} = 0.76$ was found (within the experimental uncertainty) to be equal to N_{Cu-O1}, which indeed supports the consistency of our assignment. Multiple scattering (MS) paths involving the coordination shell and the central atom are well-known sources of complication in the analyses of the EXAFS spectra at long distances but they should not play a major role here because: (i) the contribution of the MS paths involving copper and the nitrogen atoms of the first shell should cancel out in the difference as well as the contribution of the single scattering (SS) paths; (ii) MS paths involving oxygen or chlorine atoms cannot contribute to a signal that would be as intense or even more intense than the contribution of the first shell SS path. These considerations were supported by many more simulations, which are not reproduced in this paper.

Insight into the dioxygen species that is formed in the oxygenated xerogel **XB2** can also be drawn from solution chemistry of copper(I) complexes or from a systematic review of the crystal structures of Cu–dioxygen complexes.[29,30] The oxygenation of Cu^I complexes can generate three types of 2:1 Cu/O_2 species: an end-on *trans*-1,2-peroxodicopper(II), a side-on μ-η^2:η^2-peroxodicopper(II) and a bis(μ-oxo)dicopper(III) complex. The nature of the species that forms is primarily dictated by the denticity of the ligand.[30] In particular, the oxygenation of Cu^I complexes of sterically unhindered tetradendate tripodal ligands exclusively produces μ-1,2-peroxo complexes. Beyond denticity, other factors such as chelate ring size, nature of the donor atoms, electronic effects, steric demands and geometry are secondary in most cases. It appears that the internuclear distance R_{Cu-Cu} found for xerogel **XB2** would be significantly longer than the Cu···Cu distances in side-on dinuclear μ-η^2:η^2-peroxo copper complexes but shorter than in the end-on dinuclear *trans* μ-η^1:η^1-peroxo copper complex of Karlin et al.[31] ($R_{Cu-Cu} = 4.36$ Å). A side-on conformation should be ruled out for two reasons: (i) each dioxygen molecule would contribute to four equivalent Cu–O1 bonds and the signal at 1.86 Å should thus be twice as intense as what we found; (ii) for a coplanar side-on conformation, there is a limit ($R_{Cu-Cu} \approx 3.6$ Å) beyond which the four equivalent Cu–O1 bonds would split into two groups of unequal distances: $R_{Cu-O1} \leq R_{Cu-O2}$ and the end-on arrangement gains a higher probability.

Because no Cu/O_2 intermediate has been characterized, upon oxygenation in solution, for a tetrasubstitued cyclam copper(I) complex, one has to rely on comparisons with other tetradendate systems. In this regard, the aliphatic tetraamine ligands derived from tris(2-aminoethyl)amine (tren) are considered as good models of the immobilized cyclams although the former are not macrocyclic.[33–35] These ligands form μ-1,2-peroxodicopper(II) species, and accordingly, it is more likely that the reaction of xerogel **XB1** and dioxygen leads to the formation of an end-on μ-1,2-peroxodicopper(II) complex, in conformity with the EXAFS results. Yet, the Cu–Cu distance of 4.0 Å, shorter than in structurally characterized μ-1,2-peroxodicopper(II) complexes, suggests a distorted arrangement of the peroxo moiety.

We may then raise the subsidiary question whether there is any additional information available in the difference spectrum that could give us some indication about R_{Cu-O2}. We wish to underline that the following exercise is far more speculative than the previous assignments of the Cu···O1 and Cu···Cu signatures. We tried to assign the single scattering contribution of the second oxygen to the (next) most intense peak of the FT difference spectrum, i.e. to a signal peak at $R_{Cu-O2} \approx 2.96$ Å. One could find a few arguments supporting this very speculative assignment: (i) the signal had the expected phase for a Cu···O shell; (ii) this signal also shows up in the FT spectrum of xerogel **XB2** displayed in Figure 1(A) and, thus, cannot be an experimental artefact; (iii) to remain consistent with $R_{Cu-Cu} \approx 4$ Å, we have added the constraint: $R_{Cu-O2} \leq 3.02$ Å, but steric hindrance from the carbon atoms of the *N*-propyl groups would make distances $R_{Cu-O2} \leq 2.7$ Å very unlikely. A tentative estimation of the Cu–O1–O2 angle is possible only if we assume that the distance $d_{O1-O2} = 1.432$ Å as in the end-on peroxo structure of Karlin et al.[31] To a first approximation, one would calculate a bent angle Cu–O1–O2 of 127.7° to be compared with 108° in the structure of Karlin et al.[31] Recall that Kitajima et al.[20] predicted that, for pentacoordinate copper sites, the end-on dinuclear μ-η^1:η^1-peroxo-like structure should be the most favorable structure with Cu–O–O angles of the order of 130°. Our speculative assignment of the signal peaking at ca. 2.96 Å to the Cu···O2 single scattering path had another geometrical implication in that the distance Cu···Cu would be too short to enable the sequence of four atoms {Cu1···O1···O2···Cu2} be coplanar. From elementary 3D geometry considerations, we found that the directions of the Cu1–O1 and Cu2–O2 bonds should be rotated by ca. 93° with respect to each other. This would be required to minimize the steric hindrance between the two macrocyclic ligands.

We have implicitly suggested so far that dinuclear sites {Cu1;Cu2} should pre-exist in the oxygen-free xerogel **XB1**. Supporting arguments were found in the EXAFS spectra recorded at the Cl K-edge. The Cl K-edge FT spectra $\mathrm{Im}\tilde{\chi}_N(R)$ of the oxygen-free and oxygenated xerogels **XB1** and **XB2**, respectively, are shown in Figure 2(A) whereas difference FT spectra of the virtual species [**XB1**-**XB2**] are displayed in Figure 2(B). Here, the optical FT spectra were systematically corrected using the phase shifts and scattering amplitudes of a Cl···Cu shell. We carefully checked the consistency of our E_0 value with respect to earlier analyses of other model compounds involving Cl···Metal distances. At short distances, there are unbalanced contributions of Cu^I sites and pentacoordinate Cu^{II} sites with well-resolved signatures peaking at: $R_{Cl-Cu^I} = 2.11 \pm 0.03$ Å, and $R_{Cl-Cu^{II}} = 2.44 \pm 0.03$ Å, respectively. Interestingly, we also found a well-defined signal at a long distance: $R_{Cl-Cu} \geq 2.71 \pm 0.03$ Å which seems to agree with our suspicion

that the Cl^- ions could asymmetrically bridge the copper sites.

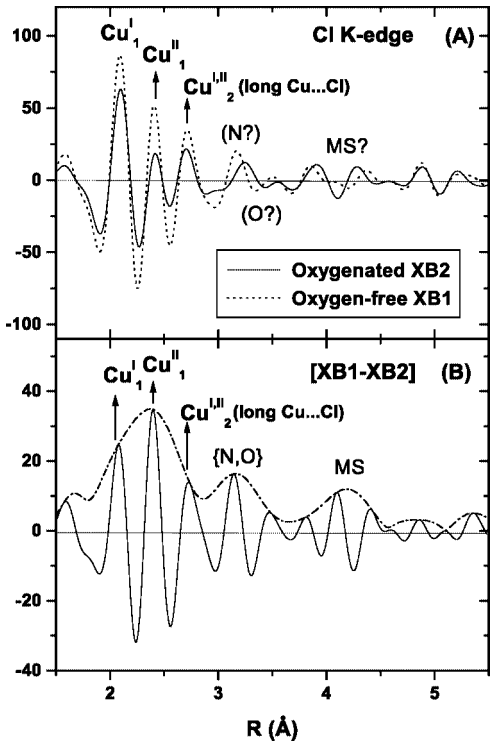

Figure 2. (A) Comparison of the Cl K-edge FT EXAFS spectra $Im\tilde{\chi}(R)$ of xerogel **XB2**[$CuCl_2$]/O_2 (solid line) and of xerogel **XB1**[$CuCl_2$]/N_2 (dotted line). Arrows mark the expected Cl···Cu distances for Cu^I–Cl and Cu^{II}–Cl bonds. The signal at 2.7 Å would be consistent with a Cl anion bridging mixed-valence $\{Cu^I,Cu^{II}\}$ sites. (B) Cl K-edge FT spectra $Im\tilde{\chi}(R)$ (solid line) and $|\tilde{\chi}(R)|$ (dot-dashed line) of the difference EXAFS signal of [**XB1** (oxygen-free) – **XB2** (oxygenated)].

Thus, we were led to seriously consider the existence of mixed-valence Cu^I and Cu^{II} sites. Note that the long distance $R_{Cl–Cu_2}$ looks quite comparable with distances (e.g. 2.674–2.707 Å) reported for chloride ions bridging mixed-valence dinuclear $\{Cu^I,Cu^{II}\}$ sites.[36] Such distances are, however, only slightly shorter than the distances (2.71–2.76 Å) found for chloride ions symmetrically bridging two Cu^{II} sites in copper hydroxychloride minerals[21,23,24] (e.g. atacamite). Cl K-edge EXAFS data are not accurate enough to discriminate between these two structural options. However, from the estimated Cu1···Cu2 distance in the deoxy-xerogel **XB1** ($R_{Cu1–Cu2} \approx 3.89$ Å), one would predict the bridging angle Cu1–Cl–Cu2 to be either 97° or 105° depending on whether Cu1 is taken as a Cu^I or a pentacoordinate Cu^{II} site. This compares rather well with the bridging angle (92°) reported for chloride ions in mixed-valence dinuclear $\{Cu^I,Cu^{II}\}$ sites.[36]

Concentrating on the FT spectrum of the oxygenated xerogel **XB2**, we found [Figure 2(A)–2(B)] only a modest amplitude reduction of the Cu^I–Cl signal while the signature of the pentacoordinate Cu^{II}–Cl site vanished completely. This rather astonishing result was confirmed a posteriori by re-investigating the Cu K-edge FT difference spectra. From Figure 1(B) we identified a positive peak at $R_{Cu^{II}–Cl} \approx 2.44$ Å together with a poorly resolved side-peak at $R_{Cu^I–Cl} \approx 2.10$ Å. There might still be an additional signal correlated with the long Cl··Cu2 distance ($R_{Cu–Cl} \approx 2.7$ Å) but it would be interfering with the signal, which we had previously assigned to the Cu1···O2 signature. These various Cu···Cl signatures are expected to appear as positive peaks in the FT difference spectrum of [**XB2-XB1**] as a consequence of the difference in the phase shifts of oxygen and chlorine scattering atoms. As far as we are concerned, the main interest of this exercise was essentially to probe the self-consistency of our assignments in the difference analyses.

At this stage, we tried to summarize in Figure 3 the possible structures of the Cu sites in the active xerogels. According to our analyses, up to four different Cu sites could coexist in xerogels **XB1** and **XB2**. In Figure 3(A), we sketched what a dinuclear site corresponding to the dioxygen adduct in **XB2** could look like. There is probably a small shift (≈ 0.2 Å ?) of the Cu atoms out of the average nitrogen plane and, most likely, also a trigonal distortion of the Cu^I–N bonds but there is no hope as yet of extracting this information from the EXAFS spectra. Moreover, any distortion of this type referring to the cyclam ligand should already pre-exist in the oxygen-free xerogel. From Figure 3(A), we realized that steric hindrance of the carbons (Cα) located on the same side of the cyclam as the dioxygen adduct should probably define the most stable configuration.

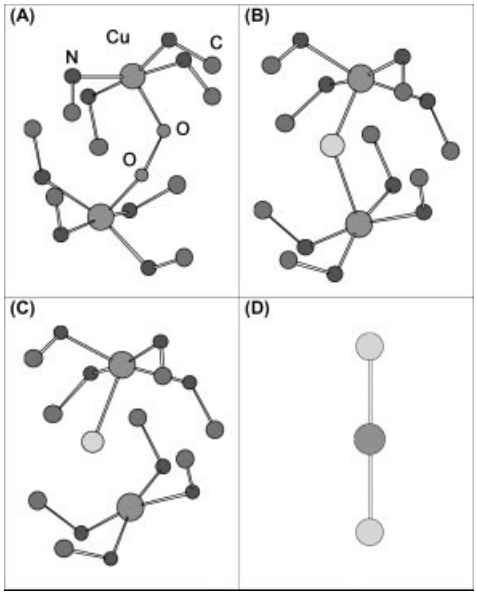

Figure 3. (A) Stereogeometry of the dinuclear μ-η^1:η^1 peroxo-like Cu site consistent with the difference EXAFS analysis with: $R_{Cu–O1}$ = 1.855 Å; $R_{Cu–O2}$ = 2.965 Å; $R_{Cu–Cu}$ = 3.988 Å. The Cu atoms were arbitrarily shifted by 0.2 Å from the average 4-N plane whereas the Cu–O bond had to be tilted by 10° with respect to the cyclam axes in order to minimize the steric hindrance of the carbons. (B) Stereogeometry of the postulated mixed-valence $\{Cu^I,Cu^{II}\}$ dinuclear site in xerogel **XB1**. (C) Stereogeometry of tetra- and pentacoordinate Cu^{II} sites coexisting only in xerogel **XB1**. (D) Linear counterion [Cl---Cu^I---Cl] identified in species **6**.

With regards to the oxygen-free xerogel, a dinuclear site in which a chloride ion would bridge two pentacoordinate copper atoms with a formal valence of 1.5 would be unstable since the system would spontaneously evolve towards configurations sketched in Figure 3(B) and (C). The dinuclear configuration of Figure 3(B) would be most convincing for a mixed-valence $\{Cu^{I},Cu^{II}\}$ species, i.e. with a pentacoordinate Cu^{I} site, a short Cu^{I}–Cl bond (2.11 Å) and a long distance Cl–Cu^{II} (2.7 Å). In the configuration of Figure 3(C), the Cu^{II} site would be pentacoordinate with the intermediary bond length $R_{Cu^{II}–Cl} \approx 2.44$ Å and the bare, tetracoordinate Cu^{I} site could easily be oxidized. Dynamic exchanges between configurations (B) and (C) would require only a small translation of the bridging chlorine atom. Last but not least, EXAFS cannot rule out at this stage the presence of linear anions $[Cl{-}{-}{-}Cu^{I}{-}{-}{-}Cl]^{-}$ [Figure 3(D)] as discussed for complex **6** (see Supporting Information).

Building on these considerations, we have generated a simulated spectrum, which approaches the experimental Cu K-edge FT difference spectrum of Figure 1(B) reasonably well. Indeed, we do not pretend that the structural problem has been solved but, at least, we come up with a model that is consistent with all EXAFS analyses. For convenience, we assumed that the signals observed at $R \approx 3.15$ Å could be assigned to the shortest intermolecular distance Cu2···C′α3. The parameters defining the scattering paths contributing to the simulated difference spectrum displayed in Figure 1(B) are listed in Table S1 of the supporting information section. The contribution of the MS paths was found to be marginal in this exercise.

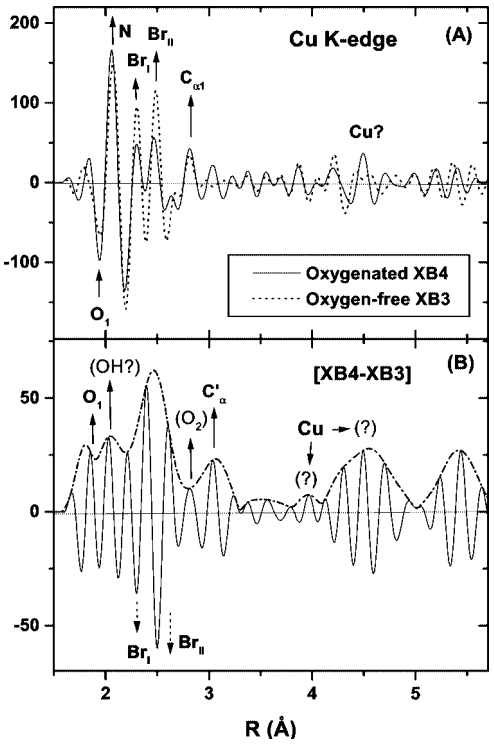

Figure 4. (A) Comparison of the Cu K-edge FT EXAFS spectra $Im\tilde{\chi}(R)$ of xerogel **XB4**$[CuBr_2]/O_2$ (solid line) and xerogel **XB3**$[CuBr_2]/N_2$ (dotted line). The split contributions of the Cu^{I}–Br and Cu^{II}–Br bonds are identified as (Br_I) and (Br_{II}). (B) Cu K-edge FT spectra Im $\tilde{\chi}(R)$ (solid line) and $|\tilde{\chi}(R)|$ (dot-dashed line) of the difference EXAFS signal of [**XB4** (oxygenated) – **XB3** (oxygen-free)]. Note the weaker amplitude of the Cu···O_1 signal.

Xerogels of Type (B) Complexed with $CuBr_2$

The Cu K-edge FT EXAFS spectra $Im\tilde{\chi}_N(R)$ of the oxygenated xerogel **XB4** and of the oxygen-free xerogel **XB3** complexed with $CuBr_2$ are compared in Figure 4(A). The FT difference spectra of the virtual species [**XB4**–**XB3**] is again reproduced in Figure 4(B). On comparing the FT spectra displayed in Figure 1(A) and Figure 4(A), it would appear that the peak assigned to the Cu···N distances is less intense and slightly shifted towards long distances in the xerogels complexed with $CuBr_2$, the average bond length increasing from 2.02Å to ca. 2.06 Å. In the FT spectrum of the oxygen-free xerogel **XB3**, there is clear evidence that bromine atoms are present in the coordination shell of copper and a refined EXAFS analysis suggested that two different Cu–Br bond lengths should be envisaged. The shortest one ($R = 2.30 \pm 0.02$ Å) would again fall very close to the Cu–Br bond length of the linear anion[37] $[Br{-}{-}{-}Cu^{I}{-}{-}{-}Br]^{-}$ and would be shorter than the Cu–Br bond length[38] in $[Cu^{I}–Br_3]^{2-}$; the long distance ($R = 2.49 \pm 0.02$ Å) would be typical of a pentacoordinate Cu^{II} complex.[39] These two resolved signals were identified as Br_I and Br_{II} in Figure 4(A) and Figure 4(B). Thus, there is again a strong indication that mixed-valence $\{Cu^{I},Cu^{II}\}$ sites[40–42] could be present in these xerogels, the signature of the Cu^{I} site being definitively less intense than the signature of the Cu^{II} site.

Independent chemical tests had previously established that the capability of xerogel **XB3** to fix dioxygen was rather poor as compared to xerogel **XB1**. This could be correlated with our observation that the difference FT spectrum of Figure 4(B) exhibits only a very weak signal at the short distance $R_{Cu–O1} = 1.86$ Å where we expect the characteristic signature of the formation of the same end-on dinuclear μ-η^1:η^1-peroxo structure discussed in the previous section.

It should be noted that the difference signals in Figure 4(B) are much less intense than in Figure 1(B). Also, the situation looks more confusing at further distances where the signature at $R_{Cu–Cu} = 3.99$ Å is now very weak whereas new signatures show up at 4.2–4.5 Å. This is not completely unexpected since: (i) the amount of dinuclear peroxo-like complex is certainly heavily reduced; (ii) we would have been suspicious if we had found the same internuclear Cu···Cu distance for the oxygen-free xerogels complexed either with $CuBr_2$ (**XB3**) or with $CuCl_2$ (**XB1**). Anyhow, the signals that show up at 4.2–4.5 Å are weak on the scale of Figure 1(B) and we clearly approach the noise limit of difference analyses.

Nevertheless, one may question why the structural changes between xerogels **XB4** and **XB3** should be so small. One could speculate that, in the presence of trapped water molecules, the dioxygen adduct would be partly and irreversibly decomposed to yield $Cu^{I,II}$–OH bonds (1.87/2.00 Å), with the OH^{-} anions replacing the released bromide anions. This would explain the presence of imperfectly

resolved signatures at 1.86/1.99 Å in Figure 4(B). Note that one would also expect longer Cu···Cu distances if there is no more bridging Br^- anion.

Inactive Xerogels Complexed with $CuCl_2$

The FT spectra $Im\tilde{\chi}_N(R)$ of the inactive xerogel **XA1** and of the oxygen-free, active xerogel **XB1** are now compared in Figure 5A. The strong signal peaking at 2.002 Å in the FT spectrum of **XA1** is most likely to be assigned once again to Cu···N distances. If one assumes that this peak refers to the average R_{Cu-N} bond length, then the corresponding bond length would be shorter than in the active xerogel **XB1** ($R_{Cu-N} \approx 2.022$ Å) and also much shorter than in model compound **6** or in its silylated precursor ($R_{Cu-N} \approx 2.13$ Å). In EXAFS, a shorter bond length is most often correlated with a stronger intensity but, quite paradoxically, the intensity of the Cu···N signal in the inactive xerogel **XA1** is reduced by ca. 30% with respect to xerogel **XB1**. In fact the intensity of the Cu···N peak is similar to the intensity of the Cu···N peak in **6** in which we pointed out the role of a destructive interference. The FT spectrum of xerogel **XA1** exhibits a well resolved negative signal peaking at 2.28 Å which one might be tempted to assign to a Cu···Cl distance. Unfortunately, such a speculative assignment would not make any sense because all crystal structures reported so far show that in pentacoordinate Cu^{II} complexes the Cu–Cl bond length is of the order of $R_{Cu-Cl} \approx 2.44$–2.47 Å as discussed earlier and illustrated by model compound **6**. There are still signatures in the FT spectrum of **XA1** which could be perfectly assigned to Cu···Cα1 and Cu···Cα2 single scattering paths and would indicate that the copper atoms are coordinated to the cyclam although the conformation of the macrocyclic ligand is certainly not the same as in the active xerogels.

We suspect that, in xerogel **XA1**, the EXAFS signal of the Cu···N distances are heavily distorted by destructive interferences within the coordination polyhedron. The negative side-lobes of the Cu···N peak are anomalously small and distorted which fuelled our suspicions. In a desperate attempt to recover some structural information lost in destructive interferences, we tried to display in Figure 5(B) the difference spectra of the virtual species [**XA1-XB1**] and [**XA1-XB2**]. The rather strong intensity of the signatures found in the FT difference spectrum of [**XA1-XB1**] confirms that the copper environment is fundamentally different in these two xerogels but, at this stage, a detailed interpretation of the difference spectrum is hopeless. If we restrict ourselves to the coordination shell, we may conjecture that there should be at least two additional signatures interfering with the Cu···N signal in the EXAFS spectrum of the inactive xerogel **XA1**: (i) the first one peaking at ca. 1.9 Å looks most typical of Cu···OH distances; (ii) the second one peaking at ca. 2.15 Å might well reflect a distortion of the cyclam macrocycle resulting in two sets of Cu···N bond lengths, e.g. 2.03 Å and 2.15 Å. It has been pointed out a while ago by Barefield and Wagner[6] that macrocycles with tertiary amines such as tetramethylcyclam could accommodate a sixth ligand at short distance with a significant folding of the macrocycle resulting in two pairs of nonequal Cu–N bonds. Such an interpretation could perhaps be consistent with the FT difference spectra of Figure 5(B). However, this is one interpretation amongst several. At a purely speculative level, we also considered the case of a dinuclear copper site now bridged with two OH^- anions. This model would explain why xerogel **XA1** could not bind anymore dioxygen. The present EXAFS study was nevertheless worth the time and effort involved: (i) it gave the experimental proof that xerogels **XA1** and **XB1** have fairly different local structures; (ii) and also that subtle changes in the coordination geometry of the cyclam would yield strong Cu···N residual signatures around 2.0(3) Å in the FT difference spectra. A contrario, the latter point supports the consistency of our difference analysis of xerogels **XB1** and **XB2**.

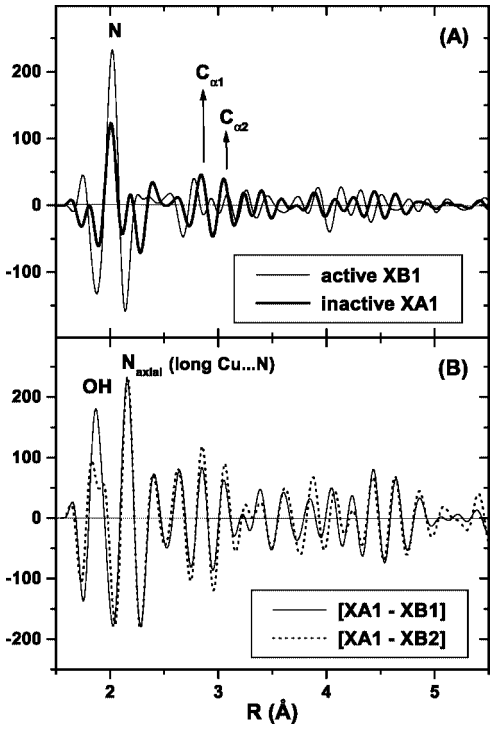

Figure 5. (A) Comparison of the FT spectra $Im\tilde{\chi}(R)$ of the inactive xerogel **XA1**[$CuCl_2$]/air (thick line) and active xerogel **XB1**[$CuCl_2$]/N_2 (solid line). Note the poor intensity of the (distorted) Cu···N signal of the inactive xerogel **XA1**. (B) FT spectra $Im\tilde{\chi}(R)$ of the difference EXAFS of [**XA1** (inactive) – **XB1** (oxygen-free)] (solid line) and of [**XA1** (inactive) – **XB2** (oxygenated)] (dotted line). Note the well-resolved contributions of the interfering signatures assigned to additional Cu···O and Cu···N single scattering paths.

Valence and Ligand Field Information

XANES Spectra as Fingerprints

We have regrouped in Figure 6(A) the deconvoluted Cu K-edge XANES spectra of all active xerogels, i.e the oxygen-free xerogels **XB1**[$CuCl_2$] or **XB3**[$CuBr_2$] and the oxygenated species **XB2**[$CuCl_2$]/O_2 or **XB4**[$CuBr_2$]/O_2. We have also added, on the same plot, the Cu K-edge XANES spectrum of the inactive xerogels **XA1**[$CuCl_2$]/Air. All spectra

were recorded over the same energy range and were deconvoluted with the same parameters (i.e. ΔE_G; ΔE_L). Therefore, there is no extra difficulty in comparing deconvoluted spectra. Noticeably, the Cu K-edge XANES spectra of all active xerogels have the same morphology. The most characteristic features were labeled from (A) to (F). Quantitative information regarding the peak energy and relative intensity of the near-edge features (A)–(E) are summarized in Table 2S (supporting information section). Most striking is the very sharp "white line" (C) peaking at 8985.33 eV, the intensity of which decreases by only ca. 15% in air or dioxygen. In all XANES spectra, there is a shoulder labeled (D) which peaks at 8987.4 eV. It is particularly well resolved in the spectra of xerogels **XB1**[$CuCl_2$] and **XB2**[$CuCl_2$]. Much weaker but still quite real are the pre-edge structures (A) and (B) found at 8980.4 eV and 8983.3 eV, respectively. In the case of the inactive xerogel **XA1**, the white line (C) is not only shifted towards high energy but its intensity is reduced in the ratio 3:1 whereas the shoulder (D) seems to become progressively smaller.

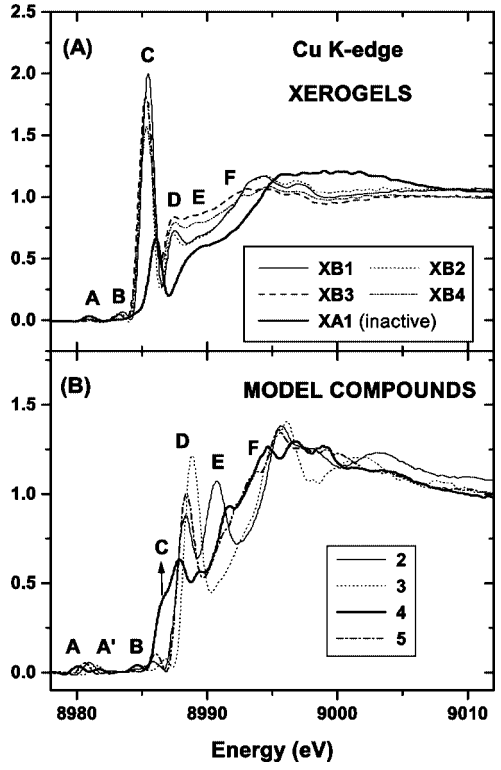

Figure 6. Numerically deconvoluted Cu K-edge XANES spectra. (A) XANES spectra of active xerogels: **XB1**[$CuCl_2$]/N_2; **XB2**[$CuCl_2$]/O_2; **XB3**[$CuBr_2$]/N_2 and **XB4**[$CuBr_2$]/O_2. The XANES spectrum of the inactive xerogel **XA1**[$CuCl_2$]/Air is also shown for comparison. The strong pre-edge resonance (C) is a characteristic feature of all XANES spectra of active xerogels. (B) Note the absence of any sharp resonance (C) in the Cu K-edge XANES spectra of various $[Cu(cyclam)]^{2+}$ complexes with variable coordination geometries: **2** = $Cu(cyclam)(ClO_4)_2{\cdot}0.5H_2O$; **3** = $[Cu(tmc)](BF_4)_2$; **4** = $[Cu(tmc)Cl](BF_4)$; **5** = $[Cu(dmdpc)](BF_4)_2$.

The Cu K-edge XANES spectra of model compounds **2**–**5** were regrouped in Figure 6(B). Clearly, the XANES spectra of tetra-, penta- or hexacoordinate cyclam complexes are quite different. The case of the pentacoordinate complex **4** is particularly relevant here since it was found to exhibit a marked analogy with the XANES spectrum of freshly prepared samples of the silylated precursor. We wish to stress that the sharp white line (C) is very weak in the XANES spectrum of such a pentacoordinate Cu^{II} complex.

The Cl K-edge XANES spectra of the oxygen-free xerogel **XB1** and of the oxygenated sample **XB2** are shown in Figure 7(A). We included on the same plot the Cl K-edge XANES spectrum of **6** which, according to the EXAFS study, should be a pentacoordinate complex of Cu^{II} contaminated with some fraction of the linear anion $[Cl{-}{-}{-}Cu^{I}{-}{-}{-}Cl]^{-}$. It immediately appears from Figure 7(A) that the morphology of the Cl K-edge XANES spectra of xerogels **XB1** and **XB2** is similar. Interestingly, the modest intensity of the pre-edge resonance labeled "A" peaking at 2819 eV in the case of complex **6** is very weak in the case of the active xerogels.

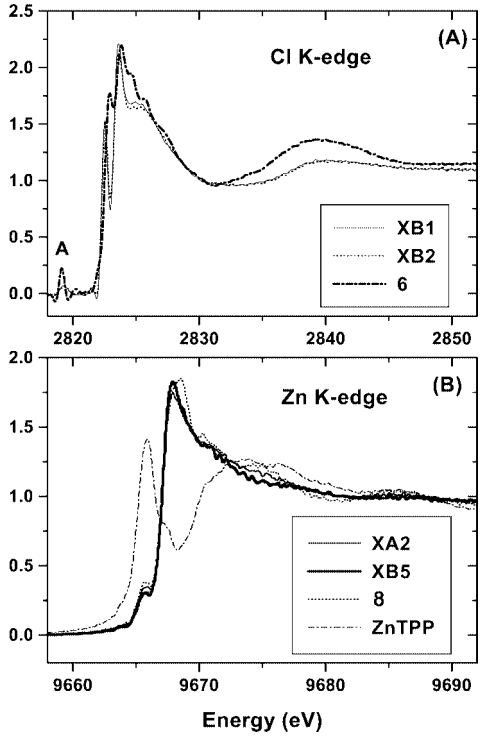

Figure 7. (A) Deconvoluted Cl K-edge XANES spectra of the active xerogels **XB1**[$CuCl_2$]/N_2 and **XB2**[$CuCl_2$]/O_2. The Cl K-edge XANES spectrum of the mixed-valence $\{Cu^{I},Cu^{II}\}$ complex **6** is also shown. It exhibits only a weak pre-edge resonance (A) at 2819 eV that vanishes for Cu^{I} compounds. (B) Deconvoluted Zn K-edge XANES spectra of xerogels **XA2**[$ZnCl_2$]/Air, **XB5**[$ZnCl_2$]/Air and of the zinc complex **8**. The XANES spectrum of Zn(TPP) was added as a reference.

This resonance was reported by Hedman et al.[43] to reflect the amount of ligand character in the antibonding orbital $(1 - \alpha^2)^{1/2}(Cu\ 3d_{x^2-y^2}) - \alpha(Cl\ 3p)$ of Cu^{II} compounds. In Cu^{I} compounds as well as in the linear anion $[Cl{-}{-}{-}Cu^{I}{-}{-}{-}Cl]^{-}$, this resonance should become much weaker because the Cu 3d orbitals should become nearly filled just as in the case of the Zn 3d orbitals of $ZnCl_2$. Figure 7(A) would thus confirm that the copper atoms in xerogels **XB1** or **XB2**

could hardly be "standard" Cu^{II} sites, as already anticipated from their EXAFS spectra.

The Zn K-edge XANES spectra of xerogels **XA2**[$ZnCl_2$], **XB5**[$ZnCl_2$] and of the silylated zinc complex **8** are displayed in Figure 7(B). The XANES spectrum of the zinc porphyrin Zn(TPP) was included as a reference. Substituting $ZnCl_2$ for $CuCl_2$ yields xerogels of type (A) and (B) that may still be slightly different but the differences in their XANES spectra become much more subtle. Here the XANES spectra of the xerogels are dominated by a single, sharp white line peaking at 9669 eV. The very weak pre-edge shoulder is consistent with a limited contribution of 3d atomic orbitals of Zn to the empty excited states. Obviously there seems to be a much stronger charge transfer from the metal to the porphyrin dianion in the case of Zn(TPP).

Simulation of XANES Spectra

In the previous section, the XANES spectra were used as sensitive fingerprints of the coordination geometry and electronic structure of the Cu sites in the xerogels. One may wonder whether ab initio simulations could help us to correlate quantitatively the observed changes with the electronic structure and the geometrical arrangement of the cyclam units. We will concentrate on two questions: (i) can we reproduce the very sharp, intense resonance (C) peak at 8986.8 eV? (ii) can we find any reliable indication that Cu^{I} sites exist in xerogels of type (B)? This is important because there is no known example of dioxygen reversibly bound to true Cu^{II} sites. We compare in Figure 8(A), Figure 8(B) and Figure 8(C), the deconvoluted experimental XANES spectra of model compounds **1**, **2** and **5** with simulated XANES spectra calculated with the MSW option of the code FDMNES, i.e. using muffin-tin potentials and the Xα functional density for exchange correlation. In each case, the geometry of the molecular cluster is systematically shown.

For the copper porphyrin **1**, we used the same muffin-tin radii as Case and Karplus[44] who already stressed that the ground state, formally written as Cu^{II} ($3d^9$) could easily transform into Cu^{I} ($3d^{10}$) by charge transfer excitation. As illustrated with Figure 8(A), the agreement between the deconvoluted experimental spectrum and our simulation looks encouraging. The simulated spectrum of Figure 8(A) reproduces the strong pre-edge resonance which was found to be highly sensitive to the charge transfer from the aromatic pyrrole towards the copper atom. The best agreement with the experimental results was obtained from the following occupation of the valence atomic orbitals: [Cu $3d^{9.40}$, $4s^{0.20}$; N $(2s2p)^{4.97}$; $C_{pyrrole}$, C_{meso} $(2s2p)^{4.10}$, C_{phenyl} $(2s2p)^{3.98}$] whereas the muffin-tin zero had to be adjusted to $V0_{imp}$ = –16.0 eV. It is not surprising that the MS calculation cannot reproduce the relative amplitudes and linewidths of the various shape resonances (especially beyond the edge) because the deconvolution is not perfect, whereas the FDMNES code takes into account only the real part of the Hedin–Lundqvist exchange-correlation potential but not its imaginary part.

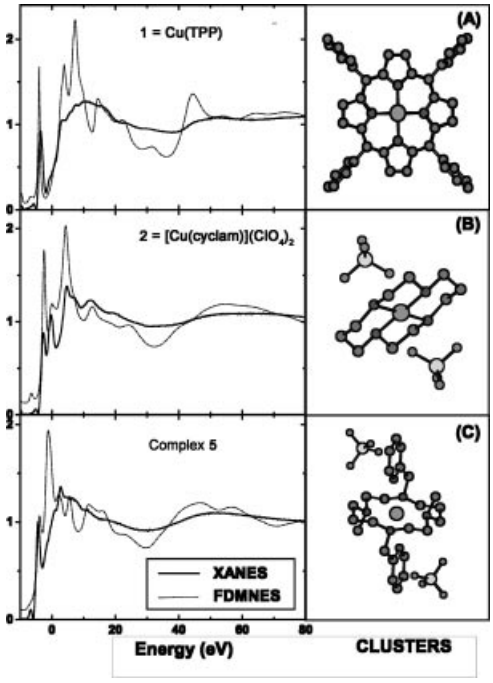

Figure 8. MSW simulations of the XANES spectra of model compounds: (A) **1** = Cu(TPP); (B) **2** = [Cu(cyclam)]$(ClO_4)_2$·0.5H_2O; (C) **5** = [Cu(dmdpc)]$(BF_4)_2$. Deconvoluted experimental spectra are shown again for comparison.

As illustrated with Figure 8(B) and Figure 8(C), our simulations of the XANES spectra of complexes **2** and **5** also look rather encouraging. Here, we expect a different charge delocalization because the cyclam macrocycles are neutral whereas the porphyrin macrocycle is a dianion. We kept the same muffin-tin radii as for the simulation of the copper porphyrin but we changed the occupation of the valence atomic orbitals. Since the crystal structure of species **2** is unknown, we incorporated the crystal structure of **2′** = [Cu(cyclam)]$(ClO_4)_2$, in which the two perchlorate anions are only very weakly bound at long distances, into our calculation. Nevertheless, Figure 8(B) reveals that the simulated XANES spectrum of species **2′** is very similar to the experimental spectrum of complex **2** which implies that **2** is most likely tetracoordinate. We used the following occupancy of the valence atomic orbitals: [Cu $3d^{9.46}$, $4s^{0.26}$; N $(2s2p)^{4.74}$; O_{axial} $(2s2p)^{6.40}$], the muffin-tin zero being now arbitrarily adjusted to $V0_{imp}$ = –18.5 eV. Note that the resonance doublet in the edge is remarkably well reproduced. For the hexacoordinate complex **5**, the best agreement with the experimental spectrum was obtained with the following occupation of the valence atomic orbitals: [Cu $3d^{9.72}$, $4s^{0.22}$; N_{equat} $(2s2p)^{4.64,\ 4.71}$; N_{axial} $(2s2p)^{4.92}$], the muffin-tin zero now being shifted to $V0_{imp}$ = –21.5 eV.

In contrast, we systematically failed to reproduce the XANES spectra of the xerogel **XB1**. In particular, we never succeeded in reproducing the sharp resonance (C) peaking at 8985.4 eV. These negative results led us to envisage that the XANES spectrum of xerogel **XB1** should result from two contributions; the first one being formally associated with a Cu^{I} ($3d^{10}$) site and the second one to a Cu^{II} ($3d^9$)

site. This required us to perform two consecutive calculations, i.e. one for each individual copper site. The difficulty is that we need a consistent calibration of the energy scale of these two spectra. Unfortunately, standard multiple scattering calculations are not reliable enough for such an exercise because the muffin-tin zero (V0) depends on the different occupation of the valence orbitals for a given copper site. This stimulated us to run the FDM option of the FDMNES code since no muffin-tin approximation is made, V0 will no longer be defined. In order to avoid a prohibitive computing time, we have performed a test calculation with a simplified dinuclear cluster in which the two copper atoms were asymmetrically bridged by one chlorine atom. The macrocyclic ligand surrounding each absorbing site was restricted to four nitrogen atoms and twelve α carbons. For the first calculation, the absorbing atom was the Cu^{I} site ($1s^1$; $3d^{10}$; $4s^{0.1}$; $4p^{0.2}$), the Cu^{II} site ($1s^2$; $3d^9$; $4s^{0.1}$; $4p^{0.2}$) contributing as a scattering atom; for the second calculation, the role of the two sites was exchanged. For simplicity, no screening effect was taken into account for the Cu^{I} site. With regards to the other scattering atoms, we extrapolated the population of the atomic orbitals from previous calculations, i.e. N_{equat} $(2s2p)^{4.58,4.60}$; Cl $(3s3p)^{7.84}$; C $(2s2p)^{4.04}$. The calculated atomic photo-ionization energies of the Cu^{I} and Cu^{II} sites were ε_{ii} = 9071.24 eV and 9059.964 eV, respectively.

The XANES spectra simulating the resolved contributions of equipopulated $\{Cu^{I};Cu^{II}\}$ sites are compared in Figure 9 in which we also reproduced the XANES spectrum of xerogel **XB1**. Since it is a usual trend of FDM calculations to generate sharp resonance lines, we found it preferable to numerically convolute the simulated XANES spectra with Lorentzian lineshapes centered at the Fermi energy E_F (Lorentzian half-width: Γ = 0.1–0.2 eV). The key conclusion is that resonances (A) (B), (C), (D) are most likely to be assigned to Cu^{I} sites, whereas resonances (E), (F) should involve the Cu^{II} site. We would like to emphasize that this is the first simulation in which resonance (C) could be reproduced with a strong intensity and we observed that this line would not depend so much on the internuclear distance $R_{Cu–Cu}$.

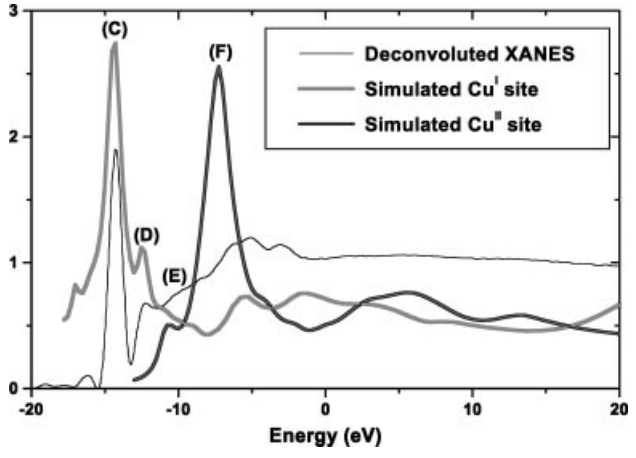

Figure 9. Simulated XANES spectra of mixed-valence $\{Cu^{I};Cu^{II}\}$ sites. The resolved contributions of the Cu^{I} and Cu^{II} sites were simulated using the *Finite Difference* option of the code FDMNES. A deconvoluted XANES spectrum of xerogel **XB1** is reproduced again for comparison. Note that resonance (C) is most likely to be assigned to the Cu^{I} site.

Conclusion

FT difference analyses at the Cu K-edge gave a strong indication that, in the oxygenated xerogel **XB2**, dioxygen would bridge two copper atoms in a kind of end-on μ-η^1:η^1 peroxo-like conformation with a short Cu–O1 distance: $R_{Cu–O1}$ = 1.855 ± 0.005 Å but with a rather long internuclear distance: $R_{Cu–Cu} \approx$ 4.0 Å. The number density $N_{Cu–O1}$ = 0.75 ± 0.1 agrees fairly well with independent measurements of O_2 adsorption (38% per copper site). There is no doubt that in both the oxygenated (**XB2**) and the oxygen-free (**XB1**) xerogels the Cu atoms are still complexed by the cyclam units. This is proved by the presence in the FT spectra of each individual xerogel of characteristic signatures assigned to the Cu···N and Cu···Cα1 single scattering paths at typical distances: $R_{Cu–N}$ = 2.02(2) Å and $R_{Cu–Cα1}$ = 2.8(8) Å, respectively. Interestingly, there is no evidence of a structural rearrangement affecting the coordination of the cyclam macrocycle in the oxygenated xerogel. This may not be so surprising if the substituted macrocycle is totally immobilized within the rigid inorganic polymeric structure of the xerogel. This could explain the reactivity of these xerogels towards dioxygen and why dioxygen is bound almost reversibly.

If we retain the model of an end-on peroxo-like conformation, then one should also observe the weaker signature of a second single scattering path at a longer Cu···O2 distance. The best we could do was to assign, in a purely speculative way, this Cu···O2 signature to a residual signal found in the difference spectrum at $R_{Cu–O2}$ = 2.9(6) Å. If this assignment is correct, then the Cu–O1–O2 angle was estimated to be ca. 128° in noticeable agreement with arguments previously developed by Kitajima et al.[20] However, we wish to underline that the corresponding deductions relative to the stereogeometry of the complex are indirect and remain speculative.

The Cl K-edge EXAFS study turned out to be particularly informative in the case of the active xerogels **XB1** and **XB2**. It established that, in the oxygen-free xerogel **XB1**, we had pentacoordinate Cu sites with both short Cu^{I}–Cl bonds ($R \approx$ 2.11 ± 0.03 Å) and typical Cu^{II}–Cl bonds ($R \approx$ 2.44 ± 0.03 Å). Chloride ions may well asymmetrically bridge dinuclear, mixed-valence copper sites as suggested by the detection in the FT spectra of a characteristic signal at a long distance ($R \geq$ 2.7 Å). We found it somewhat amazing that in the oxygenated xerogel **XB2**, the amplitude of the Cu^{I}–Cl signal decreased by ca. 20% while the signature of the pentacoordinate Cu^{II}–Cl site vanished. This result was confirmed a posteriori by the FT difference analysis at the Cu K-edge once it became possible to identify the Cu···Cl signatures. Note that the released chloride anions are most probably disordered and could hardly contribute to any detectable EXAFS signal.

Substituting $CuBr_2$ for $CuCl_2$ yields xerogel **XB3**, known to be much less reactive. Such poor activity could be correlated with a cut by ca. 50% in the intensity of the $Cu\cdots O_1$ signal (R = 1.86 Å) in the FT difference spectrum of [**XB4**-**XB3**] where **XB4** denotes the relevant oxygenated xerogel. However, we found an additional signal at $R \approx 1.98$ Å which we assigned tentatively to the Cu^{II}–OH bond of a pentacoordinate mononuclear Cu site. Inactive xerogels prepared with metallated cyclams by route (A) were also found to have a fairly different structure. It seems that a major structural change had occurred during hydrolysis and polycondensation and it was speculated that a folded conformation of the cyclam would allow the copper atom to accommodate the coordination of two OH^- anions at short distances ($R \geq 1.9$ Å) while maintaining two short ($R \approx 2.00$ Å) and two long ($R \approx 2.15$ Å) Cu–N bonds. At this stage, no refined interpretation of the EXAFS spectra of the xerogels prepared by means of route (A) is possible.

Deconvoluted XANES spectra of all xerogels prepared by route (B), i.e. by incorporating $CuCl_2$ into the hybrid xerogel, exhibit a strong pre-edge resonance at 8985.4 eV which seems to be associated with the Cu^I site of a mixed-valence $\{Cu^I,Cu^{II}\}$ structure. Simulations of the XANES spectra of a number of model compounds were carried out with the standard MSW option of the code FDMNES and gave rather encouraging results. In contrast, we systematically failed to reproduce the XANES spectrum of xerogel **XB1** using the standard MSW approach. This is not too surprising since this XANES spectrum is expected to be the superposition of the individual contributions of Cu^I and Cu^{II} sites. Unfortunately, the relative chemical shift of the Cu^I and Cu^{II} pre-edge resonances cannot be reproduced accurately enough with MSW codes relying on the crude muffin-tin approximation. A very encouraging result was nevertheless obtained using the Finite Differences option of the advanced code FDMNES. A preliminary simulation carried out beyond the muffin-tin approximation allowed us to assign unambiguously the strong pre-edge resonance (C) at 8985.4 eV to a Cu^I site.

Experimental Section

Materials: The active/inactive xerogels were complexed with $CuCl_2$, $CuBr_2$ or $ZnCl_2$:

XA1 = Xerogel type (A)[$CuCl_2$]/Air **XA2** = Xerogel type (A)[$ZnCl_2$]/air

XB1 = Xerogel type (B)[$CuCl_2$]/N_2 **XB2** = Xerogel type (B)[$CuCl_2$] + O_2

XB3 = Xerogel type (B)[$CuBr_2$]/N_2 **XB4** = Xerogel type (B)[$CuBr_2$] + O_2

XB5 = Xerogel type (B)[$ZnCl_2$]/air

All details concerning the synthesis of the metallated xerogels can be found elsewhere.[11–13] Samples **XB1**-**XB4** were handled in vacuo in tight cells and filled in glove boxes. Model compounds used as reference for the XANES or EXAFS study included: **1** = Cu(TPP); **2** = Cu(cyclam)$(ClO_4)_2\cdot 0.5H_2O$; **3**[45] = [Cu(tmc)]$(BF_4)_2$; **4**[46] = [Cu(tmc)Cl](BF_4); **5**[46] = [Cu(dmdpc)]$(BF_4)_2$; **6** = [Cu(tpc)Cl]Cl; **7** = [Cu(tpsc)Cl]Cl; **8** = [Zn(tpsc)Cl]Cl. TPP denotes the (*meso*-5,10,15,20-tetraphenylporphyrinato) macrocyclic dianion; cyclam is the 1,4,8,11-tetraazacyclotetradecane ligand; tmc refers to the 1,4,8,11-tetramethyl-1,4,8,11-tetraazacyclotetradecane macrocycle; dmdpc refers to the 1,8-dimethyl-4,11-bis(2-pyridylmethyl)-1,4,8,11-tetraazacyclotetradecane ligand; tpc and tpsc denote the 1,4,8,11-tetrapropyl-1,4,8,11-tetraazacyclotetradecane and the 1,4,8,11-tetrakis(trimethylsilylpropyl)-1,4,8,11-tetraazacyclotetradecane macrocycle, respectively.

Instruments and Methods: X-ray absorption and emission spectra were recorded with the ESRF beamline ID12.[47] The X-ray source is a helical undulator which, for the present project, was operated in the linear polarization mode. In order to scan EXAFS spectra over 2000 eV, we used the so-called "*gap-scan*" technique[48] which consists of optimizing the magnetic gap of the undulator during a scan of the monochromator in such a way that the energy of the monochromatic photons always matches the peak intensity of the undulator spectrum. The monochromator was equipped with a pair of Si (111) crystals cooled down to 152 K. The energy resolution was very close to the intrinsic limits, i.e. $\Delta E \approx 0.40$ eV at the Cl K-edge; $\Delta E \approx 1.56$ eV (1.72 eV) at the Cu (Zn)K-edges. The energy calibration was consistent with the SSRL criterion assigning the first inflexion point of the Cu foil XANES spectrum to 8980.3 eV.[49] Vertically focusing double mirrors (VFM) allowed us to keep the level of unwanted harmonics well below 5 orders of magnitude. EXAFS or XANES spectra were systematically recorded in the (integrated) Fluorescence Yield (FY) mode. Sample pellets were inserted in a vacuum-tight sample holder and were excited by the incident X-ray beam through a 12.5 μm thin Kapton window (5 mm active diameter). The sample holder (cooled down to 80 K) was itself located inside a high vacuum fluorescence chamber equipped with eight low noise photodiodes arranged in the backscattering geometry and collecting the fluorescence photons emitted over a wide solid angle. X-ray emission spectra were recorded in the spectral ranges of the Cu $K\beta_{1,3}$ (and $K\beta_{2,5}$) fluorescence lines using a high resolution spectrometer equipped with a spherically bent Si (220) crystal analyzer operated with the 440 reflection at a Bragg angle of 46.17°. The analyzer energy scale was calibrated against that of the double crystal monochromator by measuring the elastic scattering line of the reference sample **1**.

EXAFS Data Collection and Analyses: High quality Cu K-edge EXAFS spectra were recorded on model compounds **1** = Cu(TPP), **3** = [Cu(tmc)]$(BF_4)_2$ and **6** = [Cu(tpc)Cl]Cl as well as on xerogels **XA1**, **XB1**, **XB2**, **XB3** and **XB4**. For each sample, several long scans (2500 data points) were collected at low temperature (T = 80 K) over a very wide energy range [i.e. 8944–10941 eV]. No radiation damage was detected and all accumulated spectra could be averaged. EXAFS oscillations could be detected up to k = 20–22 $Å^{-1}$ in $k.\chi(k)$ spectra (Figures S1–S3 in the Supporting Information), even for the xerogels in which the metal concentration was rather low. We found a double benefit in collecting EXAFS data over a wide range in the momentum space: (i) the resolution of the FT spectra in the direct space was maximized; (ii) the identification of the signatures of heavy scattering atoms (i.e. Cu, Br or Cl) in the FT spectra by varying k_{max} in the window function was easier.

EXAFS spectra were also recorded at the Cl K-edge for xerogels **XB1** and **XB2**. The presence of a weak potassium K-edge signal at 3610 eV (associated with trace amounts of this element nonuniformly distributed over the Kapton window) in the spectra required us to truncate the $k\cdot\chi(k)$ spectra for $k \geq 14.4$ $Å^{-1}$ (see Figure S4 in the Supporting Information). A very weak argon K edge at

3200 eV was identified which was treated as a second order perturbation.

The EXAFS analyses followed standard procedures detailed elsewhere.[14] The spectra recorded in FY detection mode were systematically corrected for self-absorption.[14,50] Throughout this paper, phase and amplitude corrected "optical" FT spectra[14] were displayed. Phase shifts and backscattering amplitudes were generated using the code FEFF8.9.[51,52] Numerical fitting methods in both the direct and reciprocal spaces[14] were also available as options in our EXAFS data analysis package.

XANES: Numerical Deconvolution and ab initio Simulations: The convoluted effects of the core hole lifetime and of the finite energy resolution of the monochromator resulted in smooth but broad Voigt lineshapes, which restricted the possibility of resolving and assigning the pre-edge and shape resonances in the experimental XANES spectra. Following a strategy pioneered at the ESRF by Loeffen et al.,[53] the experimental XANES spectra were deconvoluted numerically in order to recover narrow lineshapes. The price to be paid was an artificial increase of the noise level in the XANES spectra. XANES spectra were simulated with the advanced code FDMNES which offers two options:

(i) Multiple Scattered Wave (MSW) calculations can be carried out with muffin-tin potentials spherically averaged in the atomic or outer-sphere regions but only volume-averaged in the interstitial region. In practice, the averaged muffin-tin zero ($V0_{imp}$) is a critical parameter that needs to be carefully adjusted. Muffin-tin radii can be automatically determined from standard prescriptions (e.g. using the Norman criterion[54]). Local electronic densities were obtained by superposition of atomic contributions but the Clementi–Roetti atomic wave functions[55] can be replaced by external wave functions taking into account relativistic effects (as in FEFF8.10). The occupancy of the valence orbitals can be artificially altered in order to simulate charge transfers between atoms that are no longer neutral. The Coulomb potential was then calculated by solving the Poisson equation where the energy dependent exchange-correlation potential was approximated either by a standard Xα functional density or by the real part of a Hedin–Lundqvist functional.[56]

(ii) In the finite-difference method (FDM)[57] the Schrödinger equation was solved over a grid of discrete points in a spherical volume centered at the absorbing atom. There is no need to introduce any artificial spherical symmetry or to define any interstitial region. This is most appreciable in the case of directional covalent bonding. In the present study, the lack of an arbitrarily defined muffin-tin zero was essential in order to accurately determine the contribution of Cu^{I} and Cu^{II} sites. The occupancy of the valence orbitals was artificially altered to simulate charge transfers between atoms just as in the MSW option. Unfortunately, FDM calculations resulted in a dramatic increase in computing time, which required us to perform our calculations on the powerful NEC SX-5 machine of the CNRS in Orsay (IDRIS).

Supporting Information Available (see also footnote on the first page of this article): This includes: (i) selected *raw* experimental EXAFS spectra; (ii) a detailed EXAFS study of model compounds **1**, **3** and **6**; (iii) Figure S7 illustrating the quality of the single shell fit of the Cu–O1 signal in the FT difference spectrum; (iv) Table S1 listing the parameters of scattering paths contributing to the simulated FT difference spectrum displayed in Figure 1(B); (v) a comparison of numerically deconvoluted and raw Cu K-edge XANES spectra for the model compound **1** as well as for all xerogels complexed with $CuCl_2$; (vi) Table S2 listing the peak energy and relative intensities of the resolved resonances (A)–(E).

Acknowledgments

This work is part of a joint collaboration supported by AIR-LIQUIDE and the French C.N.R.S. The allocation of 220 hours of free computing time on the NEC SX-5 machine of the IDRIS computing center in Orsay was greatly appreciated.

[1] C. K. Jørgensen, R. Reisfeld, *Struct. Bonding* **1996**, *85* (251 pages).
[2] Selected Papers on Sol-Gel for Photonics, in *SPIE Milestone Series, Vol. MS 148* (Ed.: S. I. Najafi), **1998**, 522 pages.
[3] R. J. P. Corriu, D. Leclercq, *Angew. Chem. Int. Ed. Engl.* **1996**, *35*, 1420–1436.
[4] R. J. P. Corriu, *Angew. Chem. Int. Ed.* **2000**, *39*, 1376–1398.
[5] B. Boury, R. J. P. Corriu, *Chem. Commun.* **2002**, 795–802.
[6] E. K. Barefield, F. Wagner, *Inorg. Chem.* **1973**, *12*, 2435–2439.
[7] L. Fabbrizzi, A. Poggi, *J. Chem. Soc. Chem. Commun.* **1980**, 646–647.
[8] R. Machida, E. Kimura, M. Kodama, *Inorg. Chem.* **1983**, *22*, 2055–2061.
[9] L. Fabbrizzi, M. Licchelli, P. Pallavicini, L. Parodi, *Angew. Chem. Int. Ed.* **1998**, *37*, 800–802.
[10] M. Meyer, V. Dahaoui-Gindrey, C. Lecomte, R. Guilard, *Coord. Chem. Rev.* **1998**, *178–180*, 1313–1405.
[11] G. Dubois, Ph. D. Thesis, Université de Montpellier-II **1999**.
[12] G. Dubois, R. J. P. Corriu, C. Reyé, S. Brandès, F. Denat, R. Guilard, *Chem. Commun.* **1999**, 2283–2284.
[13] G. Dubois, C. Reyé, R. J. P. Corriu, S. Brandès, F. Denat, R. Guilard, *Angew. Chem. Int. Ed.* **2001**, *40*, 1087–1090.
[14] J. Goulon, C. Goulon-Ginet, V. Gotte, X-ray Absorption Spectroscopy Applied to Porphyrin Chemistry, in: *The Porphyrin Handbook, Vol. 7* (Eds.: K. M. Kadish, K. M. Smith, R. Guilard), **2000**, 79–166.
[15] J. L. Poncet, R. Guilard, P. Friant, C. Goulon-Ginet, J. Goulon, *Nouv. J. Chim.* **1984**, *8*, 583–590.
[16] J. S. Griffith, *The Theory of Transition Metal Ions*, Cambridge University Press, Cambridge, **1961**.
[17] T. Sakurai, K. Kobayashi, H. Masuda, S. Tsuboyama, K. Tsuboyama, *Acta Crystallogr. Sect. C* **1983**, *39*, 334–337.
[18] S. Tsuboyama, K. Kobayashi, T. Sakurai, K. Tsuboyama, *Acta Crystallogr. Sect. C* **1984**, *40*, 1178–1181.
[19] K. Panneerselvam, T.-H. Lu, H. Aneetha, Y.-H. Lai, S.-C. Lin, C.-S. Chung, *Anal. Sci.* **1999**, *15*, 499–500.
[20] N. Kitajima, K. Fujisawa, C. Fujimoto, Y. Morooka, S. Hashimoto, T. Kitagawa, K. Toriumi, K. Tatsumi, A. Nakamura, *J. Am. Chem. Soc.* **1992**, *114*, 1277–1291.
[21] A. F. Wells, *Acta Crystallogr.* **1949**, *2*, 175–180.
[22] A. F. Wells, in: *Structural Inorganic Chemistry*, 4th Edition, The Clarendon Press, Oxford, **1975**, Chapter 25.
[23] A. A. Voronova, B. K. Vainshtein, *Sov. Phys. – Crystallogr.* **1958**, *3*, 445–451.
[24] A. A. Voronova, B. K. Vainshtein, *Sov. Phys. Crystallogr.* **1973**, *18*, 63–66.
[25] H. R. Oswald, Y. Iitaka, S. Locchi, A. Ludi, *Helv. Chim. Acta* **1961**, *44*, 2103–2109.
[26] M. Loos, J. Goulon, M. Bertucci, R. Bachelard, *J. Phys.* **1986**, *47*, 285–288.
[27] M. Loos, J. Goulon, M. Bertucci, R. Bachelard, *Physica B* **1989**, *158*, 188–190.
[28] M. Loos, Ph. D. Thesis, Université de Nancy-I **1990**.
[29] A. G. Blackman, W. B. Tolman, *Struct. Bonding* **2000**, *97*, 179–211.
[30] L. M. Mirica, X. Ottenwaelder, D. Stack, *Chem. Rev.* **2004**, *104*, 1013–1046.
[31] R. R. Jacobson, Z. Tyeklar, A. Farooq, K. D. Karlin, S. Liu, J. Zubieta, *J. Am. Chem. Soc.* **1988**, *110*, 3690–3692.
[32] Z. Tyeklar, R. R. Jacobson, N. Wei, N. N. Murthy, J. Zubieta, K. D. Karlin, *J. Am. Chem. Soc.* **1993**, *115*, 2677–2689.

[33] K. Komiyama, H. Furutachi, S. Nagatomo, A. Hashimoto, H. Hayashi, S. Fujinami, M. Suzuki, T. Kitagawa, *Bull. Chem. Soc. Jpn.* **2004**, *77*, 59–72.
[34] M. Becker, F. W. Heinemann, S. Schindler, *Chem. Eur. J.* **1999**, *5*, 3124–3129.
[35] M. Weitzer, S. Schindler, G. Brehm, S. Schneider, E. Hörmann, B. Jung, S. Kaderli, A. D. Zuberbühler, *Inorg. Chem.* **2003**, *42*, 1800–1806.
[36] S. R. Breeze, S. Wang, *Inorg. Chem.* **1996**, *35*, 3404–3408.
[37] J. L. Fulton, M. M. Hoffmann, J. G. Darab, B. J. Palmer, E. A. Stern, *J. Phys. Chem. A* **2000**, *104*, 11651–11663.
[38] G. J. A. A. Koolhaas, W. L. Driessen, J. Reedijk, J. L. Van der Plas, R. A. G. De Graaff, *Inorg. Chem.* **1996**, *35*, 1509–1517.
[39] F. Hanic, *Acta Crystallogr.* **1959**, *12*, 739–744.
[40] B. Scott, R. Willett, L. Porter, J. Williams, *Inorg. Chem.* **1992**, *31*, 2483–2492.
[41] J. C. Dyason, P. C. Healy, L. M. Engelhardt, C. Pakawatchai, V. A. Patrick, C. L. Raston, *J. Chem. Soc. Dalton Trans.* **1985**, 831–838.
[42] G. A. Bowmaker, P. D. W. Boyd, C. E. F. Rickard, M. L. Scudder, I. G. Dance, *Inorg. Chem.* **1999**, *38*, 5476–5477.
[43] B. Hedman, K. O. Hodgson, E. I. Solomon, *J. Am. Chem. Soc.* **1990**, *112*, 1643–1645.
[44] D. A. Case, M. Karplus, *J. Am. Chem. Soc.* **1977**, *99*, 6182–6194.
[45] C. Bucher, E. Duval, E. Espinosa, J.-M. Barbe, J.-N. Verpeaux, C. Amatore, R. Guilard, *Eur. J. Inorg. Chem.* **2001**, 1077–1079.
[46] C. Amatore, J.-M. Barbe, C. Bucher, E. Duval, R. Guilard, J.-N. Verpeaux, *Inorg. Chim. Acta* **2003**, *356*, 267–278.
[47] J. Goulon, A. Rogalev, C. Gauthier, C. Goulon-Ginet, S. Pasté, R. Signorato, C. Neumann, L. Varga, C. Malgrange, *J. Synchrotron Rad.* **1998**, *5*, 232–238.
[48] A. Rogalev, V. Gotte, J. Goulon, C. Gauthier, J. Chavanne, P. Elleaume, *J. Synchrotron Rad.* **1998**, *5*, 989–991.
[49] L.-S. Kau, J. Spira-Solomon, J. E. Penner-Hahn, K. O. Hodgson, E. I. Solomon, *J. Am. Chem. Soc.* **1987**, *109*, 6433–6442.
[50] J. Goulon, C. Goulon-Ginet, R. Cortès, J.-M. Dubois, *J. Phys.* **1982**, *43*, 539–548.
[51] J. J. Rehr, J. Mustre de Leon, S. I. Zabinsky, R. C. Albers, *J. Am. Chem. Soc.* **1991**, *113*, 5135–5140.
[52] A. L. Ankudinov, J. J. Rehr, *Phys. Rev. B* **2000**, *62*, 2437–2445.
[53] P. W. Loeffen, R. F. Pettifer, S. Müllender, M. A. Van Veenendaal, J. Röhler, D. S. Sivia, *Phys. Rev. B* **1996**, *54*, 14877–14880.
[54] J. G. Norman, *Mol. Phys.* **1976**, *31*, 1191–1198.
[55] E. Clementi, C. Roetti, *Atom. Data Nucl. Data Tables* **1974**, *14*, 177–478.
[56] L. Hedin, B. I. Lundqvist, *J. Phys. C: Solid State Phys.* **1971**, *4*, 2064–2083.
[57] Y. Joly, *Phys. Rev. B* **2001**, *63*, 125120 (10 pages).

Received: December 14, 2004
Published Online: June 7, 2005

